

Generative Data Augmentation for Object Point Cloud Segmentation

Dekai Zhu^{1,2,3}, Stefan Gavranovic², Flavien Boussuge², Benjamin Busam¹ and Slobodan Ilic^{1,2}

¹ Technical University of Munich ² Siemens AG ³ Munich Center for Machine Learning

Abstract

Data augmentation is widely used to train deep learning models to address data scarcity. However, traditional data augmentation (TDA) typically relies on simple geometric transformation, such as random rotation and rescaling, resulting in minimal data diversity enrichment and limited model performance improvement. State-of-the-art generative models for 3D shape generation rely on the denoising diffusion probabilistic models and manage to generate realistic novel point clouds for 3D content creation and manipulation. Nevertheless, the generated 3D shapes lack associated point-wise semantic labels, restricting their usage in enlarging the training data for point cloud segmentation tasks. To bridge the gap between data augmentation techniques and the advanced diffusion models, we extend the state-of-the-art 3D diffusion model, Lion, to a **part-aware generative model** that can generate high-quality point clouds conditioned on given segmentation masks. Leveraging the novel generative model, we introduce a **3-step generative data augmentation (GDA) pipeline** for point cloud segmentation training. Our GDA approach requires only a small amount of labeled samples but enriches the training data with **generated variants** and pseudo-labeled samples, which are validated by a novel **diffusion-based pseudo-label filtering** method. Extensive experiments on two large-scale synthetic datasets and a real-world medical dataset demonstrate that our GDA method outperforms TDA approach and related semi-supervised and self-supervised methods.

1. Introduction

In the past decade, 3D computer vision has made astonishing progress thanks to the advent of deep learning. One of the keys to this success lies in the abundance of annotated data. Compared with the annotation for 2D semantic segmentation, the annotation for 3D semantic segmentation is particularly time-consuming and laborious. A straightforward way to get more annotated data is to perform traditional data augmentation (TDA), which employs basic geometric transformations, like random rescaling, ro-

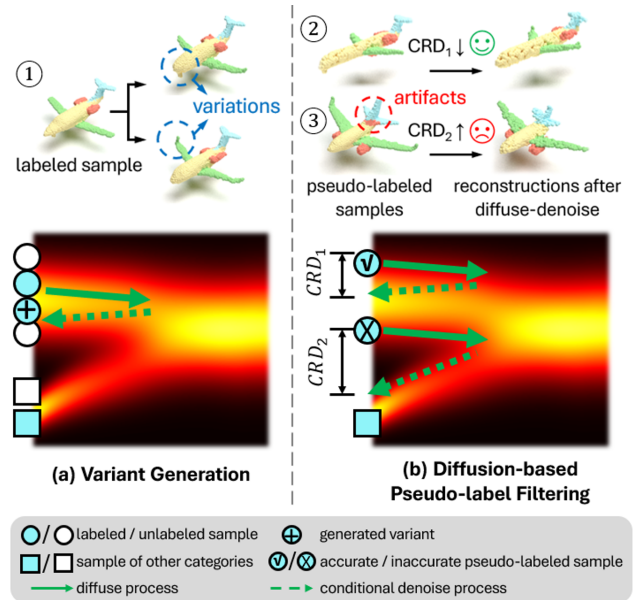


Figure 1. (a) **Variant generation** enriches the labeled data by interpolating novel samples between the existing labeled and unlabeled samples. The generated shapes exhibit diverse geometric variations. (b) **Diffusion-based pseudo-label filtering** method assesses the quality of pseudo labels based on the conditional reconstruction discrepancy (CRD), calculated by the shape deviation after the conditional diffusion-denoise process guided by the pseudo label. The sample is closely reconstructed if the pseudo label is accurate. Hence, a lower CRD indicates higher pseudo-label quality, and vice versa.

tation, flipping, jittering, etc., on already labeled data. However, this is not very useful since the variety of 3D shapes stayed small. Other approaches focused on extracting helpful information from samples with and without semantic segmentation annotations [3–6, 11, 12, 34]. These methods can be broadly classified into semi-supervised learning [12, 34], weakly-supervised learning [5, 11], and self-supervised learning [3, 4, 30, 31]. The semi-supervised method refers to annotating only a subset of samples, such as selecting 5% to 10% of available 3D objects, and training models on both labeled and unlabeled data. Weakly-supervised methods denote those that annotate only a small

number of points in each object or scene, with the most extreme case being the annotation of just one point per part, i.e., “one part, one click”. The self-supervised method initially pretrains the segmentation model on unannotated point clouds, followed by fine-tuning on a few annotated samples. These methods have achieved superior results compared to TDA techniques, but they still have limitations, such as sensitivity to the quality of pseudo labels [25].

In recent years, generative models represented by variational autoencoders (VAEs) [14], generative adversarial networks (GANs) [7], and denoising diffusion probabilistic models (DDPMs) [10] have achieved impressive performance. This provides a new perspective and can be used to bridge the gap between data annotation and data generation. This has been explored in works such as [1, 40, 46]. Experimental results in [46] demonstrate that the latest diffusion model [13] can generate high-quality samples for data augmentation in downstream 2D classification tasks, improving the prediction accuracy. However, these works focus on 2D global classification tasks, which are more straightforward than 3D segmentation tasks. Existing 3D generative diffusion models have achieved outstanding results on point cloud-based 3D shape generation [22, 42, 47]. Nevertheless, these works focus on generating 3D shapes without any part segmentation information, which cannot facilitate the training of 3D segmentation models.

Therefore, this work aims to generate high-quality 3D shapes conditioned on given segmentation annotations in cases where only a limited amount of labeled data is available. We extend the state-of-the-art point cloud generation model, Lion [42], on two levels. At the global encoding level, we integrate the statistical information of individual semantic parts into the global features, making it a more informative prior. At the local encoding level, we upgrade the original backbone PVCNN [19] to **part-aware PVCNN (p-PVCNN)**, which enables the model to learn the association between semantic part labels and point-wise geometric features, such as 3D position. Leveraging this part-aware generative model, we introduce a **3-step generative data augmentation (GDA) pipeline** that includes: **1. Semi-supervised training of the generative model.** **2. Variant generation**, which enriches the labeled dataset by interpolating novel samples between existing labeled and unlabeled samples, as depicted in Figure 1 (a). **3. Diffusion-based pseudo-label filtering**, which removes inaccurate pseudo-labeled samples. We assess pseudo-label quality using **conditional reconstruction discrepancy (CRD)**, measuring deviation after the conditional diffuse-denoise process guided by the pseudo labels, as depicted in Figure 1 (b). We conduct extensive experiments on various categories in two large-scale synthetic datasets, ShapeNetPart [39] and PartNet [24], as well as on a real-world 3D intracranial

aneurysm dataset, Intra [38]. The results confirm the superiority of GDA over TDA and related semi-supervised [12] and self-supervised [30, 31] learning methods. We validate the feasibility of GDA on various point cloud segmentation models, including PointNet [28], PointNet++ [29], Point Transformer [45] and the state-of-the-art SPoTr [27]. Additionally, we demonstrate the robustness of GDA in the challenging case where objects are arbitrarily oriented and analyze performance influencing factors of GDA, including the number of diffusion steps, the selection of hand-labeled samples, and the quality of generated labeled samples. In summary, the contributions of this work are the following:

- A novel part-aware generative model that generates point clouds conditioned on given segmentation masks.
- A novel 3-step GDA pipeline that generates labeled 3D shapes from a small portion of labeled 3D shapes and validates the quality of pseudo-labeled samples.
- Extensive experiments on two large-scale datasets and a challenging real-world medical dataset show the state-of-the-art performance of our GDA method over TDA and related semi-supervised and self-supervised methods.
- The first systematic analysis of the performance influencing factors of 3D GDA, providing valuable insights for the broader application of 3D GDA.

2. Related Works

Learning 3D segmentation from limited data. As mentioned in the last section, methods for learning from limited 3D data can be categorized into semi-supervised, weakly-supervised, and self-supervised methods.

In semi-supervised methods, only a small portion of samples are annotated. These methods leverage labeled data for supervision and use contrastive learning [35] to learn representations from unlabeled data. [12] first trains a segmentation network on labeled samples, then generates pseudo labels for unlabeled data, using predictions with high confidence to guide contrastive learning.

Weakly-supervised methods provide only incomplete annotations on each sample, e.g., sparse segmentation labels. Approaches are proposed for static objects [36], indoor [11, 20, 37] and outdoor [18] environments. These works try to propagate labels or gradients from the labeled points to their neighboring points during training by building spatio-temporal consistencies [2].

BAE-NET [4] is a representative of self-supervised methods. It transforms the segmentation problem into learning a set of indicator functions for the universal parts. ReCon [30] effectively combines contrastive learning with masked auto-encoding. More recently, Point-CMAE [31] follows this paradigm and further encourages the model to generate identical tokens when the samples are masked differently.

Diffusion-based 3D generation. DPM [22] and Point-Voxel Diffusion [47] train a diffusion model directly on point clouds, while Lion [42] achieves higher generation quality by utilizing a hierarchical VAE and latent diffusion models. More recently, [32, 41, 43, 44] focus on 3D scene generation. Due to higher semantics and geometry complexity, instead of directly generating a scene, these works rearrange indoor furniture into reasonable placements.

Generative data augmentation. While augmentation techniques based on VAEs or GANs boost performance for 3D domain adaptation [15, 16, 21], these techniques do not work equally well for GDA. Empirical results [46] show promise using diffusion models. Besides, [1, 9, 33, 40] investigate how to use diffusion models for generative data augmentation on 2D images.

3. Methodology

In this section, we first introduce DDPMs [10] and the diffuse-denoise process. Next, we improve Lion [42] at both global and local encoding levels (Figure 2) to enable it to generate labeled point clouds given segmentation masks. Based on this model, we propose a 3-step GDA pipeline for point cloud segmentation (Figure 3).

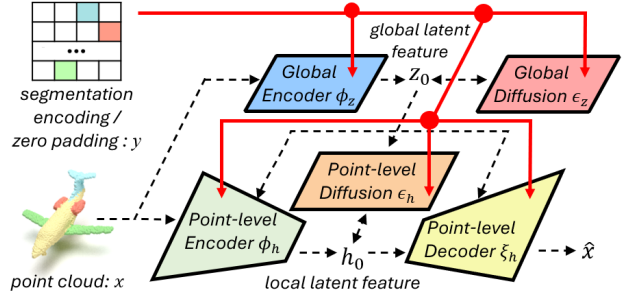
3.1. Preliminaries

Denosing diffusion probabilistic model. The diffusion model [10] generates data by simulating a stochastic discrete process: Given a sample $x_0 \sim q(x_0)$ from a distribution, the forward process gradually adds noise to the input to make it converge to a Gaussian distribution after T steps, i.e., $q(x_T) \approx \mathcal{N}(0, I)$. The training objective on the diffusion model ϵ_θ with parameters θ is to predict the noise ϵ for the perturbed sample x_t :

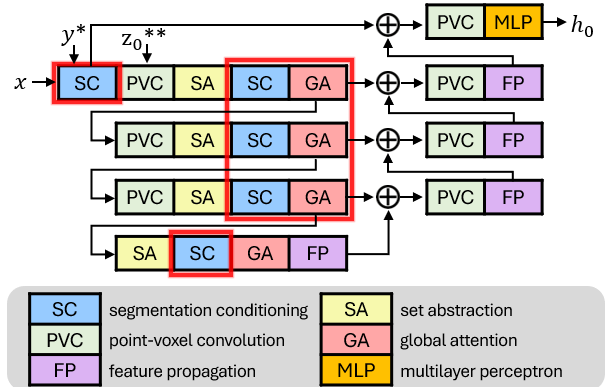
$$\mathcal{L} = \mathbb{E}_{t, x_0, \epsilon} [\|\epsilon_\theta(x_t, t, a) - \epsilon\|_2^2], \quad (1)$$

where t is the time step uniformly sampled from $\{1, \dots, T\}$, $\epsilon \sim \mathcal{N}(0, I)$ is the noise for diffusing x_0 to x_t , and a is the condition information. During inference, the diffusion model starts from a random sample $x_T \sim \mathcal{N}(0, I)$ and denoises it iteratively until $t = 0$. At each step, noise $\eta \sim \mathcal{N}(0, I)$ is added to the intermediate result x_t to increase the randomness of the denoising process.

Diffuse-denoise process. Unlike the standard inference process of DDPMs that starts from Gaussian noise and iterates for T steps, the diffuse-denoise process [23, 42] diffuses an existing sample x_0 for τ steps ($\tau < T$) and then denoises the noisy feature x_τ backwards for same steps to obtain x'_0 . During the forward diffusion process, more and more details of the input data deteriorate, while in the reverse process, besides denoising, random noise η is added to the sample at each step to increase the variety of denoised



(a) Architecture of the part-aware generative model. The extended data flows for part-awareness, highlighted in red solid arrows, show that segmentation encoding y is the input for all modules in both global and local encoding levels. Note that y is zero padding for unlabeled samples.



*: y is the input of each SC module. **: z_0 is the input of each PVC module.

(b) Architecture of p-PVCNN in the point-level encoder ϕ_h . The extended modules are highlighted in red boxes: 1. Segmentation conditioning (SC) modules are inserted in all layers to incorporate the segmentation mask y . 2. Global attention (GA) modules are used in all layers to ensure the points of small sub-parts can encode sufficient intra-part information. Note that the point-level decoder ξ_h and diffusion ϵ_h adopt a similar architecture.

Figure 2. (a) The extended Lion and (b) p-PVCNN.

samples. Therefore, the diffuse-denoise process can be utilized to synthesize different variants of a given shape.

3.2. Part-aware Generative Model

Lion [42] encodes a point cloud x to a global latent feature z_0 and local latent features h_0 (referred to as “latent points” in [42]) by using a global encoder ϕ_z and a point-level encoder ϕ_h respectively. Global and point-level diffusion modules, ϵ_z and ϵ_h , diffuse on z_0 and h_0 , while the point-level decoder ξ_h reconstructs the point cloud based on these two latent features. However, none of the modules take semantic part information into account, which hinders the generation of labeled point clouds for data augmentation in segmentation training. To address this, we introduce the segmentation label y into all modules in both global and local encoding levels, extending Lion to a part-aware generative model, as depicted in Figure 2 (a).

Global level encoding. The global encoder ϕ_z in Lion [42] utilizes the max pooling to generate the global latent feature z_0 , as in PointNet [28], while the global diffusion ϵ_z uses a stack of ResNet [8] blocks to diffuse z_0 . To incorporate the segmentation encoding y : **1.** For ϕ_z , we concatenate y with point cloud x as inputs. **2.** For ϵ_z , we first convert y into a part distribution vector $\sigma_y \in \mathbb{R}^c$ and then concatenate σ_y with z_t at step t , where c is the number of parts. σ_y represents the statistics of the number of points belonging to different parts. This distribution varies significantly among samples within the same class. For example, in the car class, a bus has a larger roof than most other cars, while a racing car lacks a roof. Thus, incorporating such an informative global prior is crucial for downstream local-level encoding. More details about the architecture the global level components are available in the supplementary materials.

Local level encoding. The point-level modules ϕ_h , ξ_h , and ϵ_h in Lion utilize a tailored 4-layer PVCNN [19] as their backbones. Each layer of PVCNN consists of point-voxel convolution (PVC) modules [19] (except the deepest layer) for local points encoding and global latent z_0 conditioning, along with set abstraction (SA) and feature propagation (FP) modules [29] for downsampling and upsampling points. Besides, a global attention (GA) module is used in the deepest layer for self-attention encoding. To incorporate the segmentation encoding y , we integrate the **segmentation conditioning module (SC)** before the PVC encoding modules in each layer. In SC modules, the segmentation encoding is concatenated with the intermediate features. This extra information brings two benefits: **1.** It reduces the uncertainty in predicting per-point geometric features, such as 3D position. **2.** It facilitates the modeling of inter-part relations, enhancing the inter-part coherence of the generated shapes. Additionally, we observe that the number of points belonging to different parts is often unbalanced on many shapes. For example, the engine part of the airplane class is relatively small and thus contains fewer points than larger parts. As the number of points decreases in deeper layers, such small-part points tend to be under-represented. To mitigate this issue, we extend the use of the GA module beyond the deepest layer, applying it across **all layers**. This ensures that points from smaller parts can encode sufficient intra-part information throughout the encoding process. The architecture of the extended **part-aware PVCNN (p-PVCNN)** is illustrated in Figure 2 (b). More details about the architecture of the local level components are available in supplementary materials.

3.3. Three-step GDA Pipeline

Leveraging the part-aware generative model, we propose a 3-step GDA pipeline for the point cloud segmentation task, as illustrated in Figure 3.

Notions. Given a training set of N labeled and M unlabeled point clouds of 3D objects ($N < M$), consisting of n points each, the learning task is to train a model to generate novel 3D shapes, represented as point clouds with associated segmentation labels. Note that the number of labeled point clouds N is significantly lower (around 10%) than the overall number of input point cloud shapes $N + M$. For N labeled point clouds, they contain the point coordinates $\mathbf{X}^L = \{x_i^l \in \mathbb{R}^{n \times 3} | i = 1, \dots, N\}$ and the one-hot segmentation encodings $\mathbf{Y}^L = \{y_i^l \in \{0, 1\}^{n \times c} | i = 1, \dots, N\}$, where c is the number of parts, e.g. the car class in ShapeNet-Part [39] contains four parts: hood, roof, wheels, and car body. For M unlabeled point clouds, they only contain the point coordinates $\mathbf{X}^U = \{x_j^u \in \mathbb{R}^{n \times 3} | j = 1, \dots, M\}$. To train the generative model with the labeled and unlabeled data in a unified manner, we use zero padding $\mathbf{Y}^U = \{y_j^u = \mathbf{0}^{n \times c} | j = 1, \dots, M\}$ for these unlabeled point clouds.

Step 1: Semi-supervised training of the generative model. Our part-aware generative model maps the point cloud $x \in \{\mathbf{X}^L, \mathbf{X}^U\}$ and associated labels or zero padding $y \in \{\mathbf{Y}^L, \mathbf{Y}^U\}$ into hierarchical latent feature spaces and diffuse on these latent features, composed of a global latent $z_0 \in \mathbb{R}^{d_z}$ and a point-level latent $h_0 \in \mathbb{R}^{n \times d_h}$, where d_z and d_h are respectively the dimensions of these two latent spaces. The training of the generative model consists of two stages. In the first training stage, we train the hierarchical VAE, consisting of the global encoder $\phi_z : \mathbb{R}^{n \times 3} \times \mathbb{R}^{n \times c} \rightarrow \mathbb{R}^{d_z}$, point-level encoder $\phi_h : \mathbb{R}^{n \times 3} \times \mathbb{R}^{n \times c} \times \mathbb{R}^{d_z} \rightarrow \mathbb{R}^{n \times d_h}$, and point-level decoder $\xi_h : \mathbb{R}^{n \times d_h} \times \mathbb{R}^{n \times c} \times \mathbb{R}^{d_z} \rightarrow \mathbb{R}^{n \times 3}$, to maximize a variational lower bound on the data log-likelihood (ELBO):

$$\begin{aligned} \mathcal{L}(\phi_z, \phi_h, \xi_h) = & \mathbb{E}_{p(x), q_{\phi_z}, q_{\phi_h}} \{ \log p_{\xi_h}(x | h_0, y, z_0) \\ & - \lambda_z D_{KL}[q_{\phi_z}(z_0 | x, y) | \mathcal{N}(0, I)] \\ & - \lambda_h D_{KL}[q_{\phi_h}(h_0 | x, y, z_0) | \mathcal{N}(0, I)] \}, \end{aligned} \quad (2)$$

where p_{ξ_h} is the prior for reconstruction prediction, q_{ϕ_z} and q_{ϕ_h} are the posterior distribution for sampling z_0 and h_0 , and λ_z and λ_h are the hyperparameters for balancing Kullback-Leibler regularization and reconstruction accuracy. In the second training stage, we train two diffusion models $\epsilon_z : \mathbb{R}^{d_z} \times \mathbb{R} \times \mathbb{R}^{n \times c} \rightarrow \mathbb{R}^{d_z}$ and $\epsilon_h : \mathbb{R}^{n \times d_h} \times \mathbb{R} \times \mathbb{R}^{n \times c \times d_z} \rightarrow \mathbb{R}^{n \times d_h}$ for z_0 and h_0 , respectively by minimizing the objectives:

$$\mathcal{L}(\epsilon_z) = \mathbb{E}_{t, z_0, \epsilon} [\|\epsilon_z(z_t, t, y) - \epsilon\|_2^2], \quad (3)$$

and

$$\mathcal{L}(\epsilon_h) = \mathbb{E}_{t, h_0, \epsilon} [\|\epsilon_h(h_t, t, [y, z_0]) - \epsilon\|_2^2], \quad (4)$$

where $z_0 = \phi_z(x, y)$, $h_0 = \phi_h(x, y, z_0)$, $x \in \{\mathbf{X}^L, \mathbf{X}^U\}$, $y \in \{\mathbf{Y}^L, \mathbf{Y}^U\}$, $\epsilon \sim \mathcal{N}(0, I)$, and t is the time step uniformly sampled from $\{1, \dots, T\}$. The models ϵ_z and ϵ_h with parameters z and h are conditioned by y and $[y, z_0]$

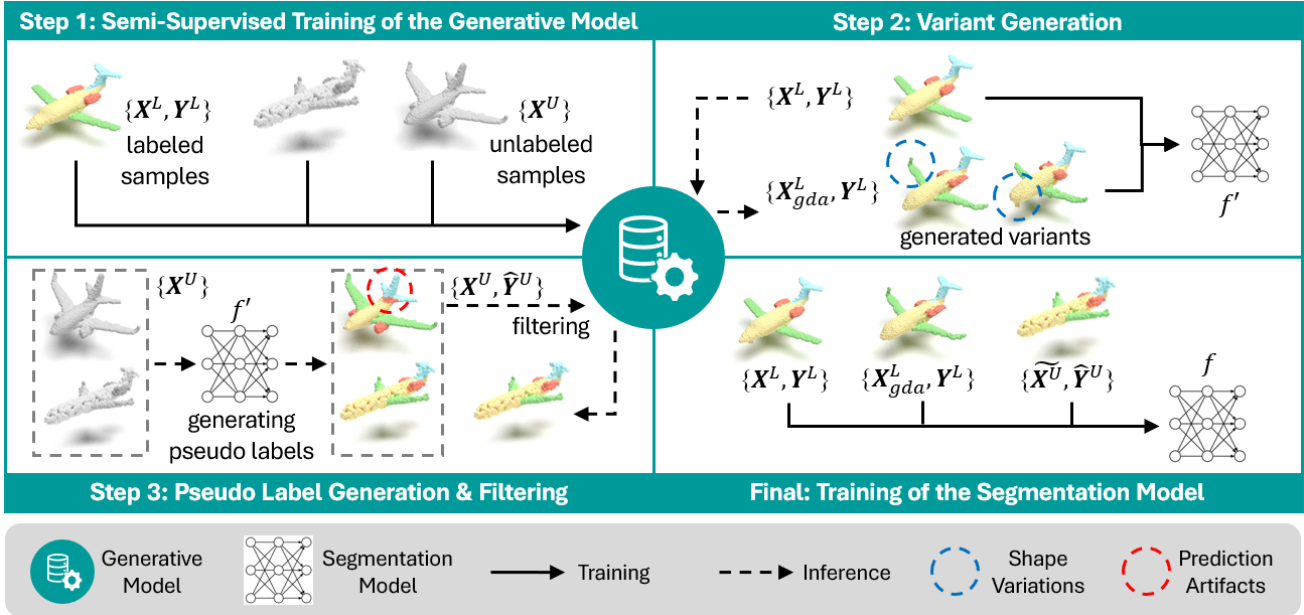


Figure 3. Pipeline of 3-step GDA. **Step 1:** Using hand-labeled samples $\{\mathbf{X}^L, \mathbf{Y}^L\}$ and unlabeled samples $\{\mathbf{X}^U\}$ to train the generative model in a semi-supervised approach. **Step 2:** Generating variants \mathbf{X}_{gda}^L by running diffuse-denoise process on \mathbf{X}^L conditioned by \mathbf{Y}^L , then using $\{\mathbf{X}^L, \mathbf{Y}^L\}$ and $\{\mathbf{X}_{gda}^L, \mathbf{Y}^L\}$ to train a temporary segmentation model f' . **Step 3:** Using f' to assign pseudo labels $\hat{\mathbf{Y}}^U$ to \mathbf{X}^U , then filtering out the low-quality pseudo-labeled samples with a large **conditional reconstruction discrepancy**. **Final:** Using hand-labeled and generated samples from step 2 & 3 to train the eventual segmentation model f . Note that the entire process is automatic, and the generated samples can be used for training various segmentation models.

respectively. The generative model is trained in this semi-supervised approach to learn the reconstruction of the point clouds with or without the segmentation labels.

Step 2: Variant generation. Once the generative model is trained, it can be used to run a τ -step diffuse-denoise process on \mathbf{X}^L . For each labeled sample x_i^l , we can obtain a set of variants $\mathbf{X}_i^l = \{x_{i,\tau}^l \in \mathbb{R}^{n \times 3} | 0 < \tau < T\}$ conditioned by the same segmentation labels y_i^l . Compared with x_i^l , the generated variants $x_{i,\tau}^l$ contain some local deformations that are learned from both labeled and unlabeled data. Thus, this process essentially performs interpolation between the existing labeled and unlabeled samples, while ensuring that the generated samples maintain a reasonable shape. An intuitive illustration is presented in Figure 1 (a), where the generated shapes exhibit diverse and reasonable variations. Through this process, segmentation annotations are properly transferred to the newly generated samples. With the original hand-labeled data \mathbf{X}^L and the novel generated variants $\mathbf{X}_{gda}^L = \{\mathbf{X}_i^l | i = 1, \dots, N\}$, we can train a temporary segmentation neural network $f' : \mathbb{R}^{n \times 3} \rightarrow \{0, 1\}^{n \times c}$ for predicting pseudo labels.

Step 3: Pseudo label generation & filtering. Using f' , we can generate pseudo labels $\hat{\mathbf{Y}}^U = \{\hat{y}_j^u \in \{0, 1\}^{n \times c} | j = 1, \dots, M\}$ on unlabeled samples \mathbf{X}^U . The pseudo labels in-

evitably contain some artifacts that can degrade the training of segmentation models. Instead of visually inspecting the pseudo-labeled samples, we propose a novel **Diffusion-based pseudo-label filtering** method to evaluate the quality of pseudo labels: **1.** The generative model performs a τ' -step diffuse-denoise process ($0 < \tau' < T$) on each unlabeled sample x_j^u , **conditioned** by their pseudo label \hat{y}_j^u . During this process, x_j^u is perturbed and then reconstructed to \hat{x}_j^u . Notably, the noise η is deprecated during denoising to reduce the randomness. **2.** We compute the deviation between x_j^u and \hat{x}_j^u to evaluate the quality of \hat{y}_j^u . If \hat{y}_j^u is accurate, the sample should be well reconstructed after this process. Otherwise, significant deviation occurs as \hat{x}_j^u adapts to the inaccurate pseudo label. We define this deviation as **conditional reconstruction discrepancy (CRD)**, where a large CRD indicates a low-quality pseudo label, and vice versa. An intuitive comparison is presented in Figure 1 (b). The airplane ②, with accurate pseudo labels, is closely reconstructed, whereas the substantial change in the engine (red) part's volume in ③ results in a large CRD, indicating the inaccuracy of its pseudo labels. CRD is calculated based on the voxelized IoU between x_j^u and \hat{x}_j^u . Specifically, we compute the IoU for each part separately and then average the results to mIoU to ensure that smaller parts are also sufficiently considered. **3.** The pseudo-labeled samples with

Method	Airplane	Car	Lamp	Motorbike	Pistol
FS	80.40	76.34	72.04	67.43	82.52
w/o aug.	76.46	70.09	66.04	56.10	77.66
only TDA	76.84	71.48	66.71	59.03	78.91
CL [12]	76.49	71.69	66.78	59.64	79.10
ReCon [30]	77.12	<u>74.51</u>	66.89	<u>65.45</u>	80.93
Point-CMAE [31]	77.46	74.45	<u>68.23</u>	65.57	<u>81.02</u>
GDA (VG)	<u>77.96</u>	72.90	66.79	61.44	80.01
GDA (VG+FP)	78.32	74.89	71.22	64.67	81.35

Table 1. Evaluation on ShapeNetPart [39]. All mIoU scores are given in percentage (%). The **best** and second-best scores for each category are highlighted in **bold** and underlined, respectively.

mIoU between x_j^u and \hat{x}_j^u below the threshold δ are filtered out.

Final: Training of the segmentation model. After 3-step GDA, the original training set only containing the hand-labeled data \mathbf{X}^L is enlarged with the generated variants $\mathbf{X}_{gda}^L = \{\mathbf{X}_i^l | i = 1, \dots, N\}$ from step 2 and the filtered pseudo-labeled samples $\tilde{\mathbf{X}}^U \subseteq \mathbf{X}^U$ from step 3. Eventually, all these labeled samples are used to train the final segmentation network $f: \mathbb{R}^{n \times 3} \rightarrow \{0, 1\}^{n \times c}$.

4. Experiments

4.1. Experimental Settings

Datasets. We conduct experiments on two large-scale synthetic datasets, ShapeNetPart [39] and PartNet [24], and a real-world dataset, IntrA [38], which contains 3d intracranial aneurysm point clouds reconstructed from MRI. We follow the official train/val/test splits of ShapeNetPart and PartNet. From ShapeNetPart, we use airplane, car, lamp, motorbike, and pistol categories, and from PartNet, we use bed, bottle, chair, faucet, and table categories. During training, 10% of the samples in each category are provided with segmentation labels, while the remaining are unlabeled. IntrA dataset contains 116 labeled and 215 unlabeled aneurysm segments. We use 24 labeled samples and 215 unlabeled samples for training, while the remaining 92 labeled samples are reserved for testing.

Segmentation network. We primarily use PointNet [28] as the segmentation model. In the ablation studies, we additionally test PointNet++ [29], Point Transformer [45], and SPoTr [27], which is a state-of-the-art and open-source model on the ShapeNetPart segmentation benchmark [26].

Methods. We evaluate the performance of the following methods in the experiments:

1. Full supervision (**FS**): using the whole training set;
2. Without data augmentation (**w/o aug.**): using 10% labeled samples without any data augmentation method;

Method	Bed	Bottle	Chair	Faucet	Table
FS	38.29	52.91	60.66	53.19	58.07
w/o aug.	27.36	40.99	51.69	40.01	46.28
only TDA	28.19	43.06	53.25	46.20	47.89
CL [12]	29.00	47.49	53.44	47.19	50.36
ReCon [30]	30.88	49.37	58.65	47.59	<u>51.02</u>
Point-CMAE [31]	<u>31.53</u>	49.54	59.23	47.26	51.17
GDA (VG)	30.69	<u>50.14</u>	56.40	<u>49.25</u>	50.22
GDA (VG+FP)	32.96	53.21	<u>58.72</u>	50.31	50.42

Table 2. Evaluation on PartNet [24]. All mIoU scores are given in percentage (%). The **best** and second-best scores for each category are highlighted in **bold** and underlined, respectively.

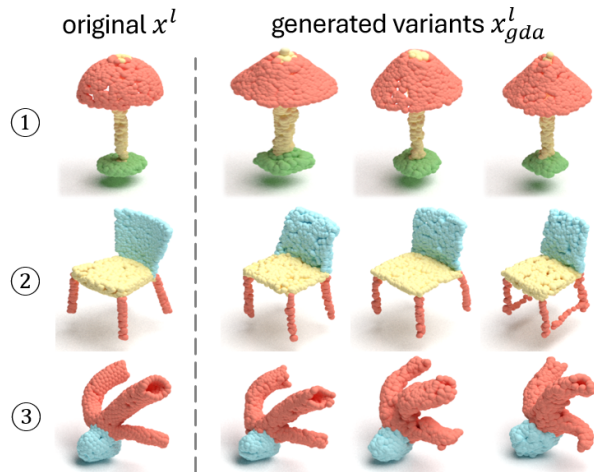


Figure 4. Illustration of hand-labeled point clouds x^l (the leftmost column) and their corresponding generated variants x_{gda}^l (the right three columns). ① A lamp from ShapeNetPart [39]. ② A chair from PartNet [24]. ③ An aneurysm segment from IntrA [38] (red: vessels, blue: aneurysm).

3. **Only TDA**: using 10% labeled samples and TDA methods, including random rescaling (0.8, 1.2), random transfer (-0.1, 0.1), jittering (-0.005, 0.005), and random flipping;

4. **Contrastive learning (CL)**: using 10% labeled samples and 90% unlabeled samples with the method in [12];

5. **ReCon**: pre-training on the whole training set without labels and fine-tuning on 10% labeled samples with the self-supervised method proposed in [30];

6. **Point-CMAE**: pre-training on the whole training set without labels and fine-tuning on 10% labeled samples with the self-supervised method proposed in [31];

7. **GDA based on variant generation (VG)**: using 10% labeled data and the generated variants \mathbf{X}_{gda}^L ;

8. **GDA based on variant generation and filtered pseudo labels (VG+FP)**: using 10% labeled samples, \mathbf{X}_{gda}^L , and the filtered pseudo-labeled samples $\tilde{\mathbf{X}}^U$. Note that TDA is used in **all** methods above except method 2.

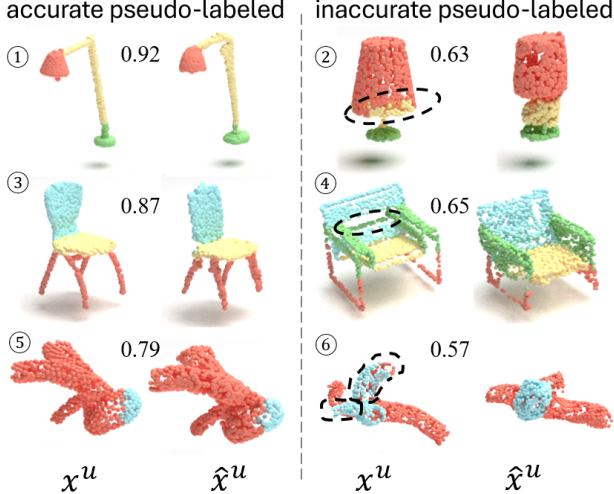


Figure 5. Illustration of the pseudo-labeled samples x^u and the reconstructed samples \hat{x}^u after the diffuse-denoise process conditioned on pseudo labels \hat{y}^u . Samples x^u with accurate \hat{y}^u are closely reconstructed, whereas those with inaccurate \hat{y}^u undergo substantial shape deviation, especially in the misclassified parts, highlighted by black dashed circles. The values represent the voxelized IoU between x^u and \hat{x}^u . A **higher** IoU indicates a **lower** conditional reconstruction discrepancy (CRD) and **higher**-quality pseudo labels, and vice versa.

Experimental Details. The training of our generative model includes two stages. The VAE modules are trained for 8k epochs in the first stage, and the latent diffusion modules are trained for 24k epochs in the second stage. An Adam optimizer with a learning rate of 1e-3 is utilized in these two stages. The parameter sizes of the VAE and diffusion modules are 22.3M and 88.9M, respectively. We set the mIoU threshold δ to 0.7 for pseudo-label filtering. For the segmentation models, we train them [27–29, 45] following the official default settings. We conduct the experiments using an NVIDIA RTX 3090 GPU with 24GB of VRAM.

4.2. Main Results

We report the experimental results of mIoU scores on ShapeNetPart [39], PartNet [24], and IntrA [38] in Table 1, 2, and 3 respectively. Across all these datasets, GDA with variant generation and filtered pseudo labels (VG+FP) achieves the best performance in most categories. On average, GDA outperforms methods using only TDA and PointCMAE [31] by **3.50%** and **0.74%** on ShapeNetPart, **5.41%** and **1.38%** on PartNet, **6.38%** and **1.46%** on IntrA dataset. Notably, PointNet trained with 10% hand-labeled data and GDA even surpasses the model trained with full supervision on the bottle class in PartNet. To prove the stability of GDA despite the stochasticity of DDPM, we repeat the experiment on car class 10 times. The results of using only TDA and GDA are **71.49±0.27** and **74.92±0.46**.

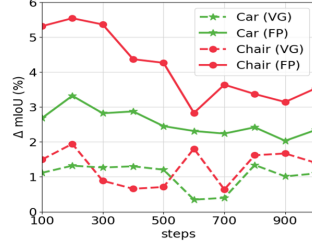


Figure 6. Impacts of the diffusion number on variant generation and pseudo-label filtering. The y-axis represents the mIoU improvement over TDA.

Method	Aneurysm
w/o aug.	37.49
only TDA	42.29
CL [12]	43.63
ReCon [30]	47.37
Point-CMAE [31]	47.21
GDA (VG)	46.85
GDA (VG+FP)	48.67

Table 3. Evaluation on IntrA [38] (no ‘FS’ since all labeled samples are used for training/test).

Figure 4 presents generated variants x_{gda}^l alongside their corresponding original samples x^l . The generated variants exhibit realistic and diverse local deformations, such as variations in lamp shades (①), chair legs (②), and healthy vessels (③), enhancing the data diversity beyond simple geometric transformations. Figure 5 illustrates the deviation in samples x^u after the diffuse-denoise process conditioned by accurate or inaccurate pseudo labels \hat{y}^u . Samples (①, ③, ⑤) with accurate pseudo labels are closely reconstructed with high voxelized IoU scores between x^u and \hat{x}^u , indicating a low CRD and the high quality of \hat{y}^u . In contrast, parts of samples (②, ④, ⑥) that are misclassified undergo substantial deviation after this process, with points being repositioned according to the corresponding prediction. This results in the low voxelized IoU between x^u and \hat{x}^u , indicating a high CRD and the low quality of \hat{y}^u . More examples of generated variants and deviations in reconstructed samples are provided in supplementary materials.

4.3. Ablation Studies

Impacts of Diffusion-based pseudo-label filtering. We use the generative model as a filter to remove samples with inaccurate pseudo labels. In this experiment, we compare our approach with other filtering methods, including: 1. Using all pseudo labels without any filtering, and 2. PseudoAugment [17], which filters out pseudo labels with low confidence scores. We conduct the experiments on the car class. The results of the above two methods are **73.13** and **73.46**, respectively, both of which are lower than the result of GDA (**74.89**).

Impacts of the number of diffusion steps. In both variant generation and pseudo-label filtering, the generative model diffuses for τ and τ' steps, respectively. During this process, increasing the number of diffusion steps enhances the diversity of regenerated samples. However, excessive diffusion steps may degrade shape quality, particularly if the generative model is not sufficiently well-trained. To analyze this effect, we conduct experiments on the car and chair cate-

Backbone	Method	Airplane	Car	Lamp	Motorbike	Pistol
PointNet++	only TDA	78.10	71.52	72.64	57.88	73.24
	[29] GDA (VG+FP)	79.92	74.66	81.15	65.27	79.53
PT [45]	only TDA	79.15	71.63	75.67	53.01	75.44
	GDA (VG+FP)	81.06	75.25	81.42	64.73	81.07
SPoTr [27]	only TDA	79.36	71.00	80.78	46.25	75.71
	GDA (VG+FP)	81.25	75.73	81.31	65.04	81.99

Table 4. GDA for PointNet++ [29], Point Transformer [45], and SPoTr [27] on ShapeNetPart [39].

Method	Airplane	Car	Lamp	Motorbike	Pistol
FS	71.98	72.71	57.53	60.59	76.99
w/o aug.	20.49	17.84	22.35	16.53	31.54
only TDA	61.12	31.09	37.56	48.38	43.82
Point-CMAE [31]	68.23	62.97	55.49	59.37	70.02
GDA (VG+FP)	70.47	67.43	57.76	58.14	71.98

Table 5. Evaluation on ShapeNetPart [39] (arbitrary orientation).

gories, varying τ from 100 to 1k steps in increments of 100. As shown in Figure 6, the variants generated with different diffusion steps consistently contribute to downstream training. Based on this observation, we incorporate samples generated across all diffusion steps in all experiments. For τ' varying from 100 to 1k steps in increments of 100, both categories achieve the best performance with 200 steps. Therefore, we adopt this setting in other experiments in this work.

GDA for various segmentation models. In this experiment, we test the performance of GDA using PointNet++ [29], Point Transformer [45], and SPoTr [27] on ShapeNetPart. The experimental results listed in Table 4 show that GDA steadily enhances the performance of these models, including the SOTA [26] model, SPoTr [27].

Objects in arbitrary orientations. Objects in ShapeNetPart are presented in canonical poses, while maintaining the pose consistency of 3D objects in real-world applications is challenging. To test the robustness of our GDA method against arbitrarily oriented objects, we randomly rotate the objects in ShapeNetPart [39] and repeat the experiments. The results listed in Table 5 show that GDA exhibits a larger advantage over TDA and Point-CMAE [31] in this challenging case, outperforming them by **20.76%** and **1.94%** respectively on average across categories.

Quality of hand-labeled and generated data. We have observed that some hand-labeled samples from ShapeNetPart [39] contain labeling errors. Therefore, in the experiments presented above, we inspect the quality of labels and exclude the problematic samples when selecting the hand-labeled samples \mathbf{X}^L for training. To evaluate the robustness

Selection	mIoU	Level	mIoU
only TDA (C)	31.09	only TDA	43.26
only TDA (w/o C)	27.53	GDA-L1	50.72
GDA (C)	67.43	GDA-L1,2	54.89
GDA (w/o C)	59.27	GDA-L1,2,3	54.96

Table 6. Impact of the quality of original labeled data (C: labeled data is selected with check).

Table 7. Impact of the quality of generated labeled data.

of GDA against label errors, we re-train a generative model on arbitrary-oriented cars while the hand-labeled samples (10%) are randomly selected. The results listed in Table 6 show that while GDA still outperforms TDA, it experiences a more substantial performance drop due to the presence of label errors. More discussions on the impacts of low-quality labeled samples on TDA and GDA are available in the supplementary materials.

Additionally, we analyze the influence of the quality of generated samples \mathbf{X}_{gda}^L on GDA. Since there is no ground truth for the generated labeled point clouds, we classify them into 3 categories based on visual inspection: (1) L1 - good quality; (2) L2 - few wrong labels or shape artifacts; (3) L3 - low-quality samples with shape distortion or wrong labels. We rate 100 samples for each category across arbitrary-oriented airplane, car, and lamp classes. The distribution of L1, L2, and L3 samples are 49/46/5, 36/50/14, and 44/49/7 for these categories, respectively. Examples of three levels are demonstrated in supplementary materials. We train the segmentation models using combinations of L1, L1+2, and L1+2+3 quality samples, respectively. The results listed in Table 7 indicate the generated samples of L1 and L2 quality steadily improve the performance of the segmentation model. Although the L3-generated samples are of lower quality, their small proportion ensures they do not adversely affect the training.

5. Conclusion

In this paper, we propose a novel part-aware generative model to produce high-quality labeled point clouds from given segmentation masks. Leveraging this model, we introduce the first diffusion-based GDA framework for 3D segmentation, which enhances training with diverse 3D variants from limited labeled data and validates pseudo labels using a novel diffusion-based pseudo-label filtering method. Experiments on three challenging datasets and various segmentation models demonstrate the robustness of GDA and its superiority over TDA and related semi-/self-supervised methods. As a pioneering work in 3D GDA, this work highlights the potential of GDA in reducing manual labeling efforts and improving segmentation performance.

References

- [1] Shekoofeh Azizi, Simon Kornblith, Chitwan Saharia, Mohammad Norouzi, and David J Fleet. Synthetic data from diffusion models improves imagenet classification. *arXiv preprint arXiv:2304.08466*, 2023. 2, 3
- [2] Lennart Bastian, Daniel Derkacz-Bogner, Tony D Wang, Benjamin Busam, and Nassir Navab. Segmentor: Obtaining efficient operating room semantics through temporal propagation. In *International Conference on Medical Image Computing and Computer-Assisted Intervention*, pages 57–67. Springer, 2023. 2
- [3] Ye Chen, Jinxian Liu, Bingbing Ni, Hang Wang, Jiancheng Yang, Ning Liu, Teng Li, and Qi Tian. Shape self-correction for unsupervised point cloud understanding. In *Proceedings of the IEEE/CVF International Conference on Computer Vision*, pages 8382–8391, 2021. 1
- [4] Zhiqin Chen, Kangxue Yin, Matthew Fisher, Siddhartha Chaudhuri, and Hao Zhang. Bae-net: Branched autoencoder for shape co-segmentation. In *Proceedings of the IEEE/CVF International Conference on Computer Vision*, pages 8490–8499, 2019. 1, 2
- [5] Mingmei Cheng, Le Hui, Jin Xie, and Jian Yang. Spnc-net: Semi-supervised semantic 3d point cloud segmentation network. In *Proceedings of the AAAI conference on artificial intelligence*, pages 1140–1147, 2021. 1
- [6] Yan Di, Chenyangguang Zhang, Chaowei Wang, Ruida Zhang, Guangyao Zhai, Yanyan Li, Bowen Fu, Xiangyang Ji, and Shan Gao. Shapemaker: Self-supervised joint shape canonicalization, segmentation, retrieval and deformation. *arXiv preprint arXiv:2311.11106*, 2023. 1
- [7] Ian Goodfellow, Jean Pouget-Abadie, Mehdi Mirza, Bing Xu, David Warde-Farley, Sherjil Ozair, Aaron Courville, and Yoshua Bengio. Generative adversarial networks. *Communications of the ACM*, 63(11):139–144, 2020. 2
- [8] Kaiming He, Xiangyu Zhang, Shaoqing Ren, and Jian Sun. Deep residual learning for image recognition. In *Proceedings of the IEEE conference on computer vision and pattern recognition*, pages 770–778, 2016. 4
- [9] Ruifei He, Shuyang Sun, Xin Yu, Chuhui Xue, Wenqing Zhang, Philip Torr, Song Bai, and Xiaojuan Qi. Is synthetic data from generative models ready for image recognition? *arXiv preprint arXiv:2210.07574*, 2022. 3
- [10] Jonathan Ho, Ajay Jain, and Pieter Abbeel. Denoising diffusion probabilistic models. *Advances in neural information processing systems*, 33:6840–6851, 2020. 2, 3
- [11] Qingyong Hu, Bo Yang, Guangchi Fang, Yulan Guo, Aleš Leonardis, Niki Trigoni, and Andrew Markham. Sqn: Weakly-supervised semantic segmentation of large-scale 3d point clouds. In *European Conference on Computer Vision*, pages 600–619. Springer, 2022. 1, 2
- [12] Li Jiang, Shaoshuai Shi, Zhuotao Tian, Xin Lai, Shu Liu, Chi-Wing Fu, and Jiaya Jia. Guided point contrastive learning for semi-supervised point cloud semantic segmentation. In *Proceedings of the IEEE/CVF international conference on computer vision*, pages 6423–6432, 2021. 1, 2, 6, 7
- [13] Tero Karras, Miika Aittala, Timo Aila, and Samuli Laine. Elucidating the design space of diffusion-based generative models. *Advances in Neural Information Processing Systems*, 35:26565–26577, 2022. 2
- [14] Durk P Kingma, Shakir Mohamed, Danilo Jimenez Rezende, and Max Welling. Semi-supervised learning with deep generative models. *Advances in neural information processing systems*, 27, 2014. 2
- [15] Alexander Lehner, Stefano Gasperini, Alvaro Marcos-Ramiro, Michael Schmidt, Mohammad-Ali Nikouei Mahani, Nassir Navab, Benjamin Busam, and Federico Tombari. 3d-vfield: Adversarial augmentation of point clouds for domain generalization in 3d object detection. In *Proceedings of the IEEE/CVF conference on computer vision and pattern recognition*, pages 17295–17304, 2022. 3
- [16] Alexander Lehner, Stefano Gasperini, Alvaro Marcos-Ramiro, Michael Schmidt, Nassir Navab, Benjamin Busam, and Federico Tombari. 3d adversarial augmentations for robust out-of-domain predictions. *International Journal of Computer Vision*, 132(3):931–963, 2024. 3
- [17] Zhaoqi Leng, Shuyang Cheng, Benjamin Caine, Weiyue Wang, Xiao Zhang, Jonathon Shlens, Mingxing Tan, and Dragomir Anguelov. Pseudoaugment: Learning to use unlabeled data for data augmentation in point clouds. In *ECCV*, pages 555–572. Springer, 2022. 7
- [18] Minghua Liu, Yin Zhou, Charles R Qi, Boqing Gong, Hao Su, and Dragomir Anguelov. Less: Label-efficient semantic segmentation for lidar point clouds. In *European Conference on Computer Vision*, pages 70–89. Springer, 2022. 2
- [19] Zhijian Liu, Haotian Tang, Yujun Lin, and Song Han. Point-voxel cnn for efficient 3d deep learning. *Advances in Neural Information Processing Systems*, 32, 2019. 2, 4
- [20] Zhengzhe Liu, Xiaojuan Qi, and Chi-Wing Fu. One thing one click: A self-training approach for weakly supervised 3d semantic segmentation. In *Proceedings of the IEEE/CVF Conference on Computer Vision and Pattern Recognition*, pages 1726–1736, 2021. 2
- [21] Adrian Lopez-Rodriguez, Benjamin Busam, and Krystian Mikolajczyk. Project to adapt: Domain adaptation for depth completion from noisy and sparse sensor data. In *Proceedings of the Asian Conference on Computer Vision*, 2020. 3
- [22] Shitong Luo and Wei Hu. Diffusion probabilistic models for 3d point cloud generation. In *Proceedings of the IEEE/CVF Conference on Computer Vision and Pattern Recognition*, pages 2837–2845, 2021. 2, 3
- [23] Chenlin Meng, Yutong He, Yang Song, Jiaming Song, Jiajun Wu, Jun-Yan Zhu, and Stefano Ermon. SDEdit: Guided image synthesis and editing with stochastic differential equations. In *International Conference on Learning Representations*, 2022. 3
- [24] Kaichun Mo, Shilin Zhu, Angel X Chang, Li Yi, Subarna Tripathi, Leonidas J Guibas, and Hao Su. Partnet: A large-scale benchmark for fine-grained and hierarchical part-level 3d object understanding. In *Proceedings of the IEEE/CVF conference on computer vision and pattern recognition*, pages 909–918, 2019. 2, 6, 7
- [25] Yassine Ouali, Céline Hudelot, and Myriam Tami. An overview of deep semi-supervised learning. *arXiv preprint arXiv:2006.05278*, 2020. 2

- [26] Papers with Code. 3d part segmentation on shapenet-part. <https://paperswithcode.com/sota/3d-part-segmentation-on-shapenet-part>, 2025. Accessed: 2025-03-06. 6, 8
- [27] Jinyoung Park, S. Lee, Si Hyeon Kim, Yunyang Xiong, and Hyunwoo J. Kim. Self-positioning point-based transformer for point cloud understanding. *2023 IEEE/CVF Conference on Computer Vision and Pattern Recognition (CVPR)*, pages 21814–21823, 2023. 2, 6, 7, 8
- [28] C. Qi, Hao Su, Kaichun Mo, and Leonidas J. Guibas. Pointnet: Deep learning on point sets for 3d classification and segmentation. *2017 IEEE Conference on Computer Vision and Pattern Recognition (CVPR)*, pages 77–85, 2016. 2, 4, 6
- [29] C. Qi, L. Yi, Hao Su, and Leonidas J. Guibas. Pointnet++: Deep hierarchical feature learning on point sets in a metric space. In *Neural Information Processing Systems*, 2017. 2, 4, 6, 7, 8
- [30] Zekun Qi, Runpei Dong, Guofan Fan, Zheng Ge, Xiangyu Zhang, Kaisheng Ma, and Li Yi. Contrast with reconstruct: Contrastive 3d representation learning guided by generative pretraining. In *International Conference on Machine Learning*, pages 28223–28243. PMLR, 2023. 1, 2, 6, 7
- [31] Bin Ren, Guofeng Mei, Danda Pani Paudel, Weijie Wang, Yawei Li, Mengyuan Liu, Rita Cucchiara, Luc Van Gool, and Nicu Sebe. Bringing masked autoencoders explicit contrastive properties for point cloud self-supervised learning. In *Proceedings of the Asian Conference on Computer Vision*, pages 2034–2052, 2024. 1, 2, 6, 7, 8
- [32] Jiapeng Tang, Yinyu Nie, Lev Markhasin, Angela Dai, Justus Thies, and Matthias Nießner. Diffuscene: Scene graph denoising diffusion probabilistic model for generative indoor scene synthesis. *arXiv preprint arXiv:2303.14207*, 2023. 3
- [33] Brandon Trabucco, Kyle Doherty, Max Gurinas, and Ruslan Salakhutdinov. Effective data augmentation with diffusion models. *arXiv preprint arXiv:2302.07944*, 2023. 3
- [34] Lingjing Wang, Xiang Li, and Yi Fang. Few-shot learning of part-specific probability space for 3d shape segmentation. In *Proceedings of the IEEE/CVF Conference on Computer Vision and Pattern Recognition*, pages 4504–4513, 2020. 1
- [35] Saining Xie, Jiatao Gu, Demi Guo, Charles R Qi, Leonidas Guibas, and Or Litany. Pointcontrast: Unsupervised pre-training for 3d point cloud understanding. In *Computer Vision—ECCV 2020: 16th European Conference, Glasgow, UK, August 23–28, 2020, Proceedings, Part III 16*, pages 574–591. Springer, 2020. 2
- [36] Xun Xu and Gim Hee Lee. Weakly supervised semantic point cloud segmentation: Towards 10x fewer labels. In *Proceedings of the IEEE/CVF conference on computer vision and pattern recognition*, pages 13706–13715, 2020. 2
- [37] Cheng-Kun Yang, Ji-Jia Wu, Kai-Syun Chen, Yung-Yu Chuang, and Yen-Yu Lin. An mil-derived transformer for weakly supervised point cloud segmentation. In *Proceedings of the IEEE/CVF Conference on Computer Vision and Pattern Recognition*, pages 11830–11839, 2022. 2
- [38] Xi Yang, Ding Xia, Taichi Kin, and Takeo Igarashi. Intra: 3d intracranial aneurysm dataset for deep learning. In *CVPR*, pages 2656–2666, 2020. 2, 6, 7
- [39] L. Yi, Vladimir G. Kim, Duygu Ceylan, I-Chao Shen, Mengyan Yan, Hao Su, Cewu Lu, Qi-Xing Huang, Alla Sheffer, and Leonidas J. Guibas. A scalable active framework for region annotation in 3d shape collections. *ACM Transactions on Graphics (TOG)*, 35:1 – 12, 2016. 2, 4, 6, 7, 8
- [40] Zebin You, Yong Zhong, Fan Bao, Jiacheng Sun, Chongxuan Li, and Jun Zhu. Diffusion models and semi-supervised learners benefit mutually with few labels. In *Proc. NeurIPS*, 2023. 2, 3
- [41] Sihao Yu, Fei Sun, Jiafeng Guo, Ruqing Zhang, and Xueqi Cheng. Legonet: A fast and exact unlearning architecture. *arXiv preprint arXiv:2210.16023*, 2022. 3
- [42] Xiaohui Zeng, Arash Vahdat, Francis Williams, Zan Gojcic, Or Litany, Sanja Fidler, and Karsten Kreis. Lion: Latent point diffusion models for 3d shape generation. In *Advances in Neural Information Processing Systems (NeurIPS)*, 2022. 2, 3, 4
- [43] Guangyao Zhai, Evin Pinar Örnek, Dave Zhenyu Chen, Ruo-tong Liao, Yan Di, Nassir Navab, Federico Tombari, and Benjamin Busam. Echoscene: Indoor scene generation via information echo over scene graph diffusion. In *European Conference on Computer Vision*, 2024. 3
- [44] Guangyao Zhai, Evin Pinar Örnek, Shun-Cheng Wu, Yan Di, Federico Tombari, Nassir Navab, and Benjamin Busam. Commonsences: Generating commonsense 3d indoor scenes with scene graphs. *Advances in Neural Information Processing Systems*, 36, 2024. 3
- [45] Hengshuang Zhao, Li Jiang, Jiaya Jia, Philip HS Torr, and Vladlen Koltun. Point transformer. In *Proceedings of the IEEE/CVF international conference on computer vision*, pages 16259–16268, 2021. 2, 6, 7, 8
- [46] Chenyu Zheng, Guoqiang Wu, and Chongxuan Li. Toward understanding generative data augmentation. *Advances in Neural Information Processing Systems*, 36, 2024. 2, 3
- [47] Linqi Zhou, Yilun Du, and Jiajun Wu. 3d shape generation and completion through point-voxel diffusion. In *Proceedings of the IEEE/CVF International Conference on Computer Vision*, pages 5826–5835, 2021. 2, 3